Response of thin lightly-reinforced concrete walls under cyclic loading

Carlos A. Blandon[a*], Carlos A. Arteta[b], Ricardo L. Bonett[c], Julian Carrillo[d], Katrin Beyer[e], João P. Almeida[e].

[a] *Department of Civil Engineering, Universidad EIA, km 2+200 variante aeropuerto JMC,Envigado, Colombia. *Corresponding autor. carlos.blandon@eia.edu.co*
[b] *Department of Civil Engineering, Universidad del Norte, Barranquilla, Colombia.*
[c] *Department of Civil Engineering, Universidad de Medellín, Medellín, Colombia.*
[d] *Department of Civil Engineering, Universidad Militar Nueva Granada, Bogotá, Colombia.*
[e] *Earthquake Engineering and Structural Dynamics Laboratory (EESD), École Polytechnique Fédérale de Lausanne, Switzerland.*

Abstract

During the last two decades, thin concrete walls have been frequently used to brace mid- to high-rise buildings in some Latin American countries. This structural system differs significantly in terms of wall geometry and reinforcement layout from traditional cast-in-place reinforced concrete wall buildings. Limited experimental data on this wall system and the absence of post-earthquake field observations make it difficult to assess whether such walls behave similarly to the walls designed according to the current local design code. The paper presents and discusses the results of an experimental program comprising quasi-static cyclic tests of four slender, thin and lightly-reinforced concrete walls with different geometrical configurations, steel properties and reinforcement layouts, which correspond to a common construction practice in Colombia. The seismic response of the specimens was assessed in terms of crack propagation and failure modes, hysteretic and backbone curves, contribution of rocking, flexural, shear and sliding components to lateral drift, stiffness degradation, and energy dissipation capacity. The results suggest that the response of these reinforced concrete walls does not meet the performance specified in the Colombian regulation if they are designed to reach the maximum lateral drift allowed by the code.

Keywords: thin wall, reinforced concrete, cold-drawn reinforcement, welded-wire mesh, lightly-reinforced slender walls.

1. Introduction

One alternative for industrialized and low-cost housing in Latin America includes concrete wall buildings using slender and thin lightly-reinforced walls which are cast conforming the architectural layout of the residential units. This construction method uses steel or aluminum modular formwork that can be assembled in different configurations. The main advantage of this method is the significant reduction of the construction time as nonstructural divisions or facades are considerably reduced or are not required. This type of buildings has been constructed in low, moderate and high seismicity regions following specifications for reinforced concrete walls defined by the Colombian Code (NSR-10) for Earthquake-Resistant Construction [1]. Provisions for concrete structures in all versions of NSR have been based on a previous version of ACI 318. The current version of the provisions for concrete structures, which updated a previous version issued in 1998, are based on the 2008 version of ACI 318 [2]. Reinforced concrete buildings designed according to the NSR-10 regulation are supposed to have the capability of reaching a maximum lateral drift of 1.43% for the design earthquake with a return period of 475 years, without collapsing and limiting the structural damage.

The walls in the structural system under discussion have several characteristics that introduce significant differences in terms of geometry and reinforcement distribution when compared to the traditional cast-in-place reinforced concrete (RC) wall buildings considered by the ACI 318 provisions. One of the main differences is the use of walls with significantly reduced thickness (t_w) that can be as low as 70 mm with a typical range between 100 and 150 mm [3]. Such reduced thickness can be specified by designers, as the code does not have an explicit minimum value for this parameter for reinforced concrete walls.

Typically, these walls only have a single curtain of web reinforcement which is spliced to started bars of 6.3 mm (#2) or 9.5 mm (#3) diameter which extend from the foundation up to the second third of the first floor height, ensuring the required lap splice length according to the code. This single curtain of reinforcement usually consists of meshes made of cold-drawn electro welded wires, which provide the minimum steel ratio required by the local regulations. To meet the ultimate flexural demand, additional reinforcement made of deformed bars are sometimes placed at the wall edges or at connections between walls. Walls with confined boundary elements are scarce or when present, the effectively confined core area is limited or non-effective because of the small available thickness [4]. Due to the architectonic and structural dual purpose of the walls, another key characteristic of this particular system is that walls are usually connected at one or both edges forming I-, T-, C-, L-shaped or any other irregular shaped cross-sections. The wall characteristics and irregularity of wall cross-sections is also typical for other countries in South America like Chile [5] and Peru [6].

Evaluation of buildings from earthquakes in Chile (2011) and New Zealand (2011) indicated that structural damage of concrete walls was associated to high axial loads, low wall area per floor, irregular element configuration and distribution and high slenderness of the walls [7, 8, 9, 10]. Even if the buildings affected during these earthquakes have different configurations with respect to the Colombian case, the observed damage indicates that the transverse slenderness of the walls at the critical section, existing in the Colombian buildings, could facilitate out-of-plane instability when subjected to seismic load reversals. Additionally, other aspects of their response associated to specific features of the local design and construction methodology are worth investigating. According to complementary studies carried out by Arteta *et al*. [3] and Arteta [11], the Colombian thin-wall archetype has low gravity axial loading (axial load ratio below 10%), non-ductile welded-wire meshes (WWM) as longitudinal and transverse reinforcement, and predominantly low longitudinal reinforcement ratio. Additional ductile bars at the edges can be observed in the reinforcement layout of some buildings but boundary elements are absent for most cases.

The laboratory experimental data and post-earthquake field observations of walls with the above characteristics is limited, especially for thin walls with a single curtain of reinforcement and M/VL_w ratios larger than two. A previous test program carried out at EPFL [12, 13] addressed the seismic response of one typical wall configuration of Colombian buildings through unidirectional and bidirectional tests on two walls of 80 mm and 120 mm thick. These tests showed that the walls could be prone to out-of-plane buckling and limited displacement capacity, below 0.7% drift ratio. However, during this latter program, only one wall configuration was considered and the longitudinal steel was significantly more ductile than typically used in Colombian construction practice. A more recent program [14, 15] focused on uniaxial tension-compression tests on a series of 12 isolated boundary elements with different thicknesses, steel reinforcement ratios, and rebar eccentricities. These tests reported the behavior of specimens representing the boundary elements, but they evidently miss the effect of the entire wall; in particular, as discussed by Rosso et al. [15], the influence of the vertical displacement profiles imposed on wall boundary elements is significantly distinct from the imposed displacement on uniaxial tests. McMenamin [16] carried out tests on several slender precast cantilever walls; however, only two of them had an M/VL_w ratio of 2.5. The height to thickness ratio was 50 and the vertical steel ratios were 1.1% and 0.6%. The former specimen presented reinforcement buckling and concrete spalling failure for a drift below 2% while the latter specimen presented reinforcement fracture failure for a drift below 1%. Both tests did not show a significant out-of-plane response. Carrillo and Alcocer [17] reported on results of quasi-static and dynamic tests of walls with H/L_w ratios varying between 0.5 and 2 and with web shear reinforcement made of a single curtain of welded-wire meshes; however, walls were tested under low axial loads that are characteristic of low-rise housing. Tomazevic et al., [18] evaluated the seismic behavior of ten (10) rectangular reinforced concrete shear-walls with H/Lw ratio of 1.4 and double curtain of wire mesh. They analyzed the influence of different parameters such as the amount and distribution of the steel and the axial load ratio on the seismic response. The amount of horizontal and vertical reinforcement varied from 0.26% and 0.38% and two axial load ratio were considered (0.07 and 0.14 $f_c'A_g$). Six unconfined specimens were tested. The specimens with unconfined boundary elements and low axial load ratio reached a maximum lateral drift of 1.0% and presented a rupture of extreme tensioned vertical reinforcement, which generated a severe strength degradation.

Although these references provide information about performance and failure modes of the tested walls, the main characteristics of these specimens have significant differences to the walls of interest in this study including axial load ratios, reinforcing steel ratios, steel mechanical properties, transverse section geometry and steel distribution among others. The lack of experimental and numerical information for the specific type of walls of interest, hinders the possibility of verifying if the available design guidelines are directly applicable to system described above, as these guidelines have been defined based on information from walls with significantly different geometrical characteristics and reinforcement arrangements [19, 20, 21, 7].

This paper shows and discusses the results of an experimental program comprising quasi-static cyclic tests of four slender and lightly-reinforced concrete thin walls with different geometrical configurations, reinforcement mechanical properties and distribution, which are representative of the type of buildings described above. The seismic response of the specimens was assessed in terms of crack propagation and failure modes, hysteretic curves, contribution of rocking, flexural, shear and sliding components to lateral drift, stiffness degradation, and energy dissipation capacity.

2. Experimental program

The experimental program comprised the tests of four reinforced concrete (RC) walls with characteristics similar to the construction practice of buildings with thin and slender RC walls with single curtain of web reinforcement. The specimens were tested under pseudo-static reversed-cyclic loading in the Structural Mechanics Lab at the EIA University in Colombia. The test setup includes a combination of axial load, shear force and flexural moment gradient that can be considered as representative of the seismic force distribution in walls within a real building designed according to the current practice in seismic regions in Colombia.

2.1 Variables of interest and specimen definition

The main characteristics of the wall specimens were defined based on the statistical analysis of a database that comprised 28 RC thin-walled buildings constructed in Colombia [3]. The buildings analyzed vary between 5 and 18 stories, with wall area densities in the longitudinal (D_l) and transverse (D_s) directions between 1.5 and 6%, with an average of 3.6% and a coefficient of variation of 0.27. The length of flanged walls carrying most of the base shear is in the range $2 \leq L_w \leq 8$ m, with a typical length of 4.5 m. The clear height of each story is 2.4 meters, with almost no variation from one structure to another. The expected gravity axial load on the walls vary between 2 and 11% of $A_g f'_c$., where A_g is the gross area of the cross-section, and f'_c is the nominal concrete strength at ground floor. All walls have distributed steel in the web and the flange. Excluding the wall edges, longitudinal steel ratio of distributed steel in the web (ρ_w) varies between $0.2\% \leq \rho_w \leq 0.7\%$, with a typical value of 0.25% (minimum code requirement). The analysis of the database also included representative values of the thickness of flanged walls, shear span ratio, steel reinforcement ratio, number of reinforcement curtains, as well as estimations of neutral axis depth from basic section analysis. Such analysis resulted in the definition of the specimen with the characteristics shown in Table 1.

Table 1. Characteristics of test specimens.

Wall	Web reinforcement		Longitudinal reinforcement at wall edge		Type of web reinforcement	Additional wall edge reinforcement	Axial load (kN)
	ρ_s(%)	d_b (mm)	ρ_b(%)	d_b (mm)			
W4	0.27	6.4	-	-	Distributed bars	None	470
W5	0.26	7.0	-	-	Electro-welded cold-drawn mesh	None	470
W6	0.27	6.4	2.53#	12.6	Distributed bars	2#12.6mm	470
W7	0.27	6.4	1.27*	12.6	Distributed bars	2#12.6mm	490

Concrete area estimated as wall thickness (100 mm) by edge length defined as 2 times the concrete cover plus the distance between 13 mm (#4) reinforcement bars which gives a total of 100 mm.

* Concrete area equal to the short flange total area (200 mm x 100 mm).

Geometry, steel layout and type of steel reinforcement were defined as the key variables to evaluate in the experimental program. Regarding the geometry, specimens W4, W5 and W6 were conceived to characterize full scale T-shaped walls with a thickness of 100 mm, length of 2.5m and clear inter-story height (H_w) of 2.4m (see Figure 1). These three walls were named sequentially following a previous experimental program [22]. The T-shaped geometry characterizes connected walls in the perpendicular direction at one wall edge, which is a predominant geometrical configurations of the construction system. The flange of the T shape walls was included to evaluate the stabilizing effect of a connecting perpendicular wall on one side and to evaluate the effect of the vertical reinforcement placed along the connecting wall in the perpendicular direction. However, the flange length and the steel included in such flanges was mainly defined considering construction limitations and the set up capacity of the laboratory and do not necessarily represent a wall of any particular length. Selected web thickness fulfills two requirements: (i) to be representative of construction in high seismicity areas in Colombia, while (ii) still being a potentially critical case for lateral (out-of-plane) instability under cyclic loading. Such instability may arise from the large unsupported length of the web and the large slenderness ratio (H_w/t_w) [12, 23, 24, 25].

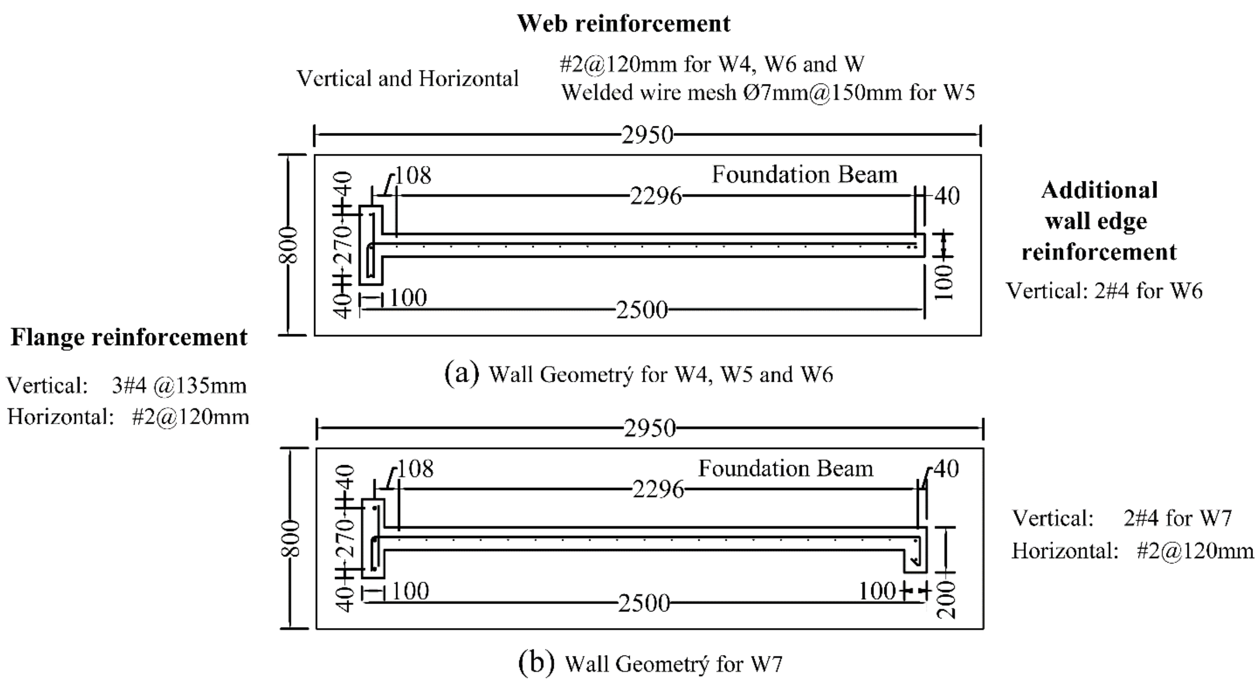

Figure 1. Geometry and reinforcement layout of the specimens.

The web of all specimens were reinforced with uniformly distributed vertical and horizontal steel. The flange was reinforced with three 12.6 mm (#4) longitudinal bars. This arrangement was of interest for this study as the additional flange reinforcement and the cross section geometry may facilitate triggering flexural-compression failures on the web edge. In addition to the distributed reinforcement described above, specimen W6 had two 12.6 mm (#4) reinforcing bars at the web edge to represent another typical construction practice for walls with larger moment demands than those represented by W4 and W5. In such case, the steel reinforcement ratio at the web is close to the minimum (0.25%) specified by ACI 318 Code [2] (e.g. $\rho_{t,W4} = \rho_{l,W4} = 0.27\%$ and $\rho_{t,W5} = \rho_{l,W5} = 0.26\%$) and the additional reinforcement at the edges is placed to provide the wall with additional strength. This additional reinforcement was also added to evaluate the potential of out-of-plane instability as this behavior is more likely to occur as the steel ratio increases. The additional steel at the edge of the web however, was defined based on the maximum test set up capacity. According to the same construction practice, the uniformly distributed reinforcement along the web is connected to the foundation using 350 mm lap splices at the wall base with 6.3 mm (#2) deformed reinforcing bars placed inside the foundation beam. The 12.6 mm (#4) bars are also lap spliced at the base using dowel bars of the same diameter and extended 700 mm inside the wall. Dowel bars are the starter reinforcement that extends from the foundation into the wall. The use of low longitudinal steel ratio along the web has been previously identified as a critical condition as it could increase the crack width and lead to prompt fracture of reinforcement in the wall section [26].

Specimen W7 had a slight geometrical variation when compared to the other specimens. It consisted in an additional short flange conforming a pseudo I-shaped section representing the case where orthogonal walls are connected at both sides of the web, which is also a common feature for this construction system. This additional flange had two 12.6 mm (#4) reinforcing bars, similar to specimen W6. The additional flange was included to evaluate a possible stabilization effect on the web edge.

Specimens W4, W6 and W7 had 6.3 mm (#2) reinforcing bars distributed along the flange and the web. The web vertical and horizontal reinforcement of specimen W5 comprised a cold-drawn welded-wire mesh (WWM). Such steel mesh is widely used as it helps reducing the construction costs and installation time [27, 28]. In fact, it is the most common reinforcement used in RC thin walls, although its non-ductile behavior is well known. Horizontal and transverse steel reinforcement ratios were kept constant for all specimens.

2.2 Tests setup and loading protocol

The test setup comprised a steel reaction frame that was braced in two orthogonal directions (Figure 2a). Loads were applied with two vertical actuators of +700 kN (-520 kN) and one horizontal actuator of +500 kN (-410 kN) of ±250 mm maximum stroke. The vertical actuators were connected to a HEA 450 steel beam, placed on a 550 mm x 350 mm reinforced concrete beam on top of the wall. The actuators were separated 2.2 m and applied the total the gravitational force (F_{vl} and F_{vr}). This force was programmed to keep an axial load ratio during the entire lateral load protocol of $0.05P/A_g f'_c$, based on a specified concrete strength of 35 MPa, Additionally, these actuators applied a variable vertical force (ΔF_v), that was slaved to the horizontal force (F_h), programmed to ensure that the value of the shear span ratio was constant ($M_b/V_b L_w = 2.08$). Larger shear span ratios up to 3.5 could be observed after the statistical analysis of the building database; however, the value selected is a representative value. Additionally, this shear span fit the maximum wall length and load capacity available in the laboratory [3]. Experimental and analytical evidence has shown that lateral displacements induce significant variations on the axial load [29, 30]; however, this variable was not evaluated in this experimental program.

The foundation beam of the walls was bolted to a strong concrete floor to avoid uplift and sliding during testing. The out-of-plane displacement of the specimen was restrained by two 150mm×150 mm×4 mm steel tubes located at both sides of the top HEA 450 beam and attached to the reactions frames (only front restraining tube shown in figure).

Once the axial load had been applied to the wall under a force-control protocol, a displacement-control protocol was implemented to apply the loading history shown in Figure 3. The load steps inducing flange compression where defined to have a positive drift. The displacement cycles were defined in terms of the horizontal yield displacement of the walls. The first yield displacement was estimated as 2.0 mm according to results of a numerical model of the wall developed using the software DIANA [31], and calibrated based on test results reported by Almeida *et al*. [13]. Cycles of 0.4 mm, 0.8 mm, 1.2 mm and 1.6 mm were defined before attaining the estimated first yield displacement of 2.0 mm. These deformation levels were to have a better evaluation of the stiffness degradation at low drift demands. The peak displacements for the next cycles were defined to achieve drift levels of 0.1%, 0.13%, 0.17%, 0.33%, 0.42%, 0.5%, 0.83%, 1.16%. The walls were subjected to two full cycles at each drift level to assess the cyclic degradation response of the walls. A slow loading velocity was chosen to disregard dynamic effects and to allow a continuous control of the instrumentation and the hydraulic system.

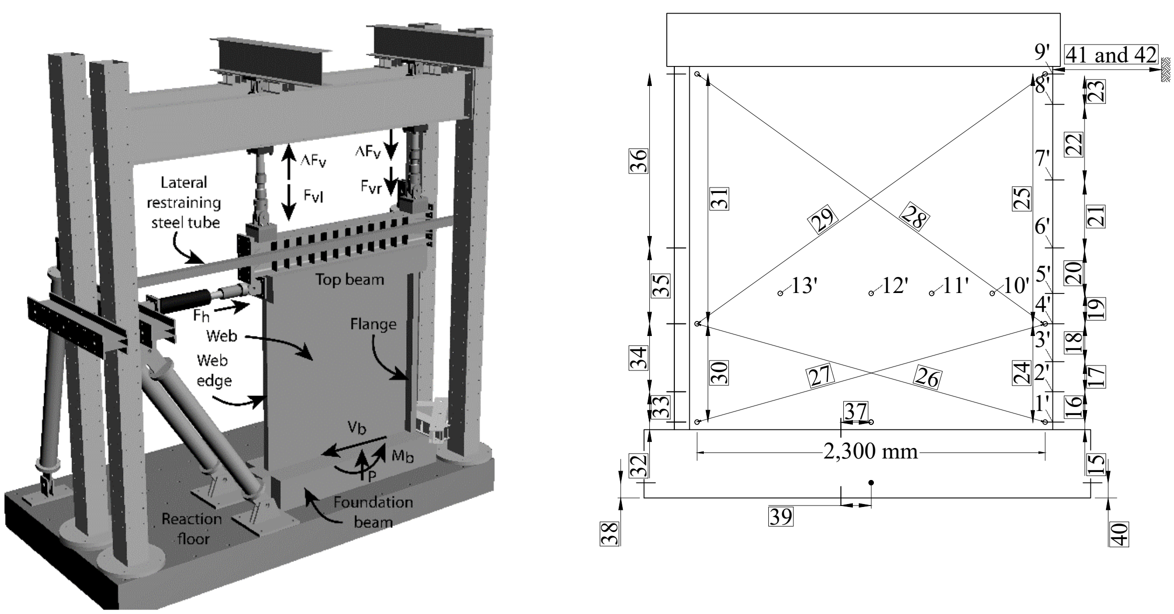

a) b)

Figure 2. Test setup: (a) experiment setup, (b) instrumentation layout and sensor numbering.

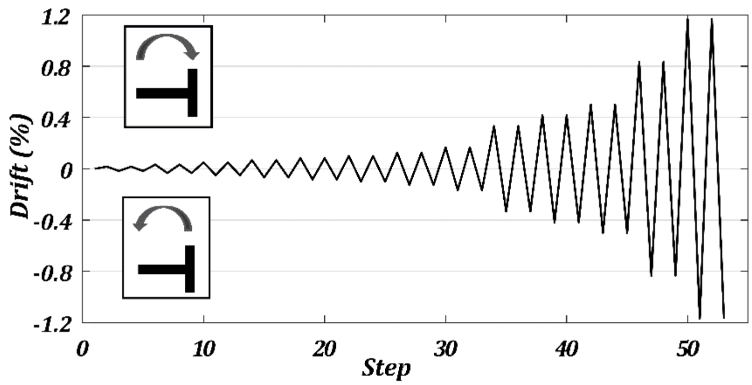

Figure 3. Loading protocol.

2.3 Instrumentation

The instrumentation scheme comprised several transducers to measure in-plane and out-of-plane deformations. Figure **Error! Reference source not found.**b shows the layout of the potentiometric displacement transducers (PDT) used to measure the contribution of sliding (37), flexural (15 to 23, 32 to 36) and shear deformations (24 to 31) to the total displacement of the wall. In addition, wire-PDTs (1' to 13') were connected perpendicularly to the wall to capture the out-of-plane displacement profile along the web edge, along its length, and at 1.2 m above the wall-foundation interface. Other sensors were installed to measure sliding (39) and uplift (38, 40) of the foundation beam. To trace the cracking pattern evolution, a random speckle pattern of high contrast was painted on the web surface of walls W5 to W7. Pictures were recorded every 30 seconds during the tests with a full-frame digital SLR camera. Images were post-processed using a digital image correlation (DIC) technique [32, 33, 34].

2.4 Mechanical properties of the materials

Specified nominal compressive strength for the concrete was 35 MPa. Actual concrete strength at the day of testing was 39.1 MPa for W4, 40.1 MPa for W5, 39.2 for W6, and 47.0 MPa for W7. The tensile stress-strain curves of the steel reinforcement measured using coupon tests are shown in Figure 4. Tensile tests of reinforcement were carried out in the Materials and Structures

Laboratory at the Nueva Granada Military University in Colombia. The yield and maximum stress for the reinforcing steel were 563 MPa and 691 MPa, respectively, for the 6.3 mm (#2) bars; 419 MPa and 630 MPa, respectively, for the 12.6 mm (#4) bars; and 723 MPa and 759 MPa, respectively, for the 7 mm-WWM.

The 12.6 mm (#4) reinforcing steel complied with ASTM-A706 standard [35] with the typical yield plateau and fracture elongation larger than 10%. However, the cold-drawn wires from the mesh and the 6.3 mm (#2) reinforcing steel exhibited a less ductile behavior, as shown in Figure 4. The stress-strain curve of the 7mm-WWM used in specimen W5 transitioned from the elastic to the plastic branch smoothly without developing a yield plateau and exhibiting a flat post-yield response, characterized by a rupture strain smaller than 3% in average (Figure 4a). The 6.3 mm (#2) bars used to reinforce the web of specimens W4, W6 and W7 did not show a defined yield plateau either, however, the steel exhibited some strain hardening and the rupture strain was approximately twice the rupture strain for the cold-drawn wire from the mesh (Figure 4b).

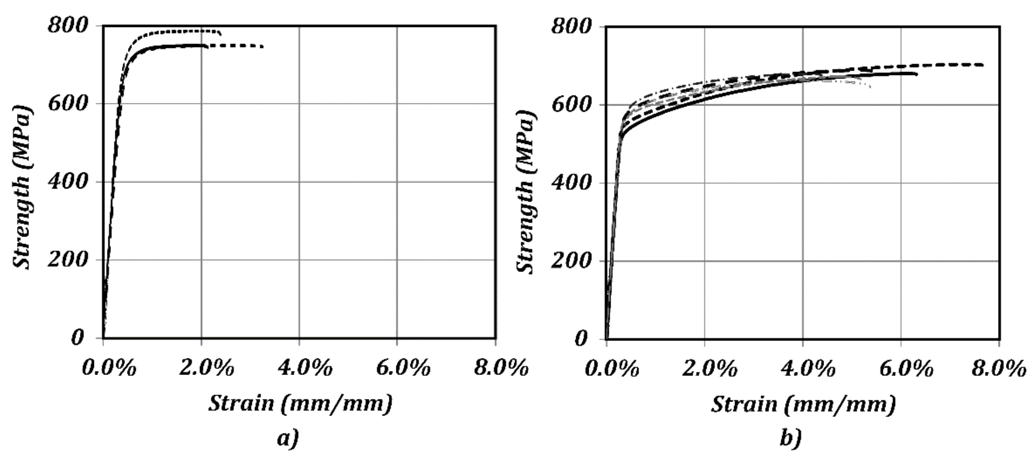

Figure 4. Stress-strain curves of steel reinforcement: (a) 7mm-diameter electro-welded wire mesh (3 samples), (b) 6.3mm-diameter (#2) deformed bars (6 samples).

3. Wall behavior

In this section, the propagation of damage of each wall specimen is evaluated in terms of its cracking patterns and failure mode. The hysteretic behavior is assessed in terms of lateral force and lateral drift ratio.

3.1 Cracking propagation and failure mode

Cracking for specimen W4 was recorded in the classical manner using markers and crack width rulers at the end of the cycles of the loading protocol. On the other hand, for specimens W5 to W7, a digital image correlation (DIC) technique was used to assess the crack evolution pattern. Cracking is described in terms of drift ratio (Δ_R). The drift ratio was computed as the quotient between the lateral displacements measured below the top beam and the height of the wall panel (2.4 m).

The cracking pattern at the end of the test of W4 is shown in Figure 5. The crack pattern that developed during the load steps inducing flange compression was significantly different to the one developed during the steps that put the flange in tension. In the first case, cracks were located along the web at three main locations, namely, at the wall foundation interface, at 0.55 m and at 1.7 m above the panel-foundation interface. When the first crack opened, the wall experienced a sudden displacement that was captured by the sensors. For the load steps inducing tension cycles, cracking was evenly distributed along the wall height (Figure 5a). Failure, defined as a lateral force drop larger than 20% of the maximum lateral force, was reached when loading during the cycle with Δ_R=0.63% in the negative direction (flange in compression), when several of the 6.3 mm (#2) dowel bars connecting the wall to the foundation fractured. When reversing the load, the concrete at the web edge started crushing followed by the fracture of the 12.6 mm steel bars of the flange at Δ_R=0.71%.

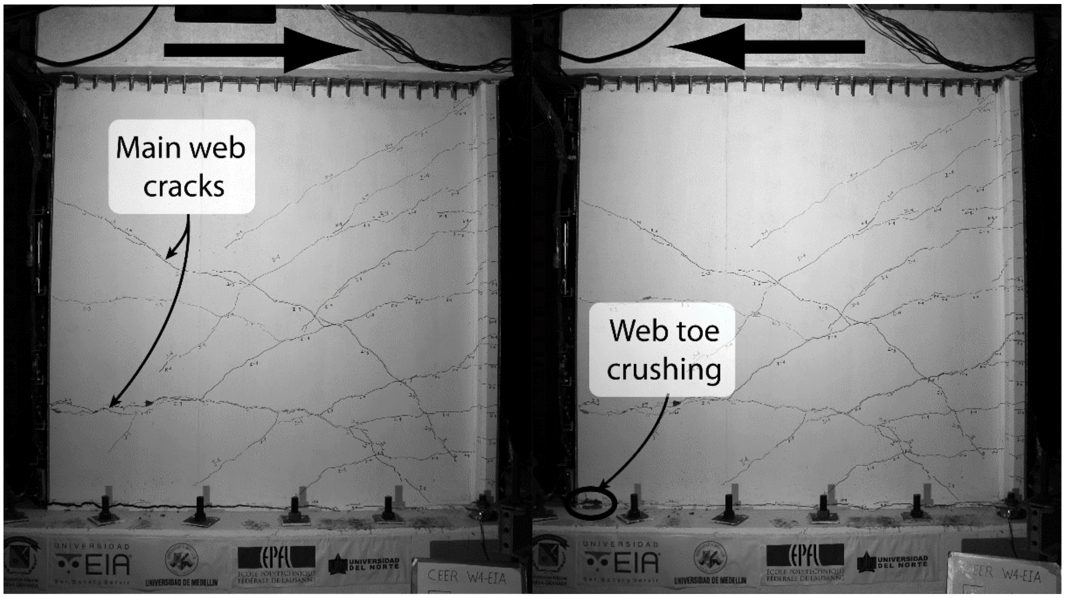

Figure 5. Cracking pattern at the end of test of specimen W4: (a) flange compression cycles (left), (b) flange tensile cycle (right).

Figure 6 shows the cracking pattern at the end of the test of specimen W5. For the direction where the flange is in compression, a crack at the wall-foundation interface was also observed, and it remained as the only significant crack during several cycles until a second horizontal crack appeared at the web edge. This second crack was located 1.2 m above the wall base. A secondary crack located at the wall-top beam interface also appeared at early cycles but it did not exhibit an apparent opening. Cracking propagation along the flange was similar to W4 as it was distributed along the entire height of the panel. The dowel bars located near the flange started fracturing at Δ_R=0.50% when compressing the web edge. A strength degradation was observed at Δ_R=0.67% when more dowel bars fractured. Spalling of the compressed web toe also occurred at the same drift level. Failure occurred due to the fracture of the 12.6 mm (#4) reinforcing bars on the flange side, at the wall foundation interface, at Δ_R=0.83% (Figure 6b).

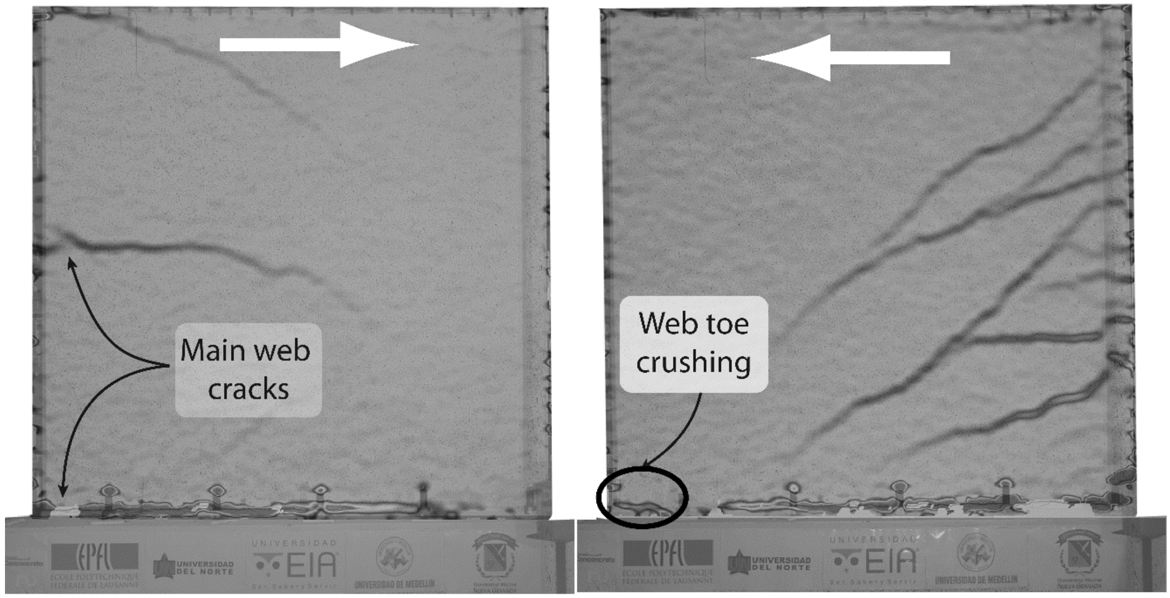

Figure 6. Cracking pattern at the end of test of specimen W5: (a) load steps inducing flange compression (left), (b) load steps inducing flange tension (right). The plot shows the vertical strains as computed by the DIC software. The patter revealed by the DIC software does not represent the crack width but a region of large strains around the crack.

Figure 7 shows the cracking pattern at the end of test W6. Cracking on the web edge side of specimen W6 was significantly influenced by the two additional 12.6 mm (#4) mm reinforcing bars. They induced a more distributed crack propagation along the entire wall height compared to specimens W4 and W5. Similarly to the other units, the largest crack was located at the wall-foundation interface. One additional crack was observed at the web edge side, 0.70 m above the base, and was associated to the lap splice of the 12.6 mm (#4) reinforcement bars, which ended at this location. Another large crack was observed at the top of the wall and it was probably associated with a stress concentration at the top beam interface. Fracture of the 6.3 mm (#2) starter bars also occurred for a drift ratio Δ_R=0.67% during the load step that induced compression in the flange. A vertical crack appeared at the web toe along the 100 mm thick wall side and continued enlarging and spreading upwards. This crack triggered a lap-splice failure of the specimen due to the slippage of the 12.6 mm (#4) reinforcing bars during the first load step of the 0.83% drift ratio that induced compression in the flange and tension in the lap splice at the web. This failure mode resembled wall lap-splice failures observed in other experimental programs [36].

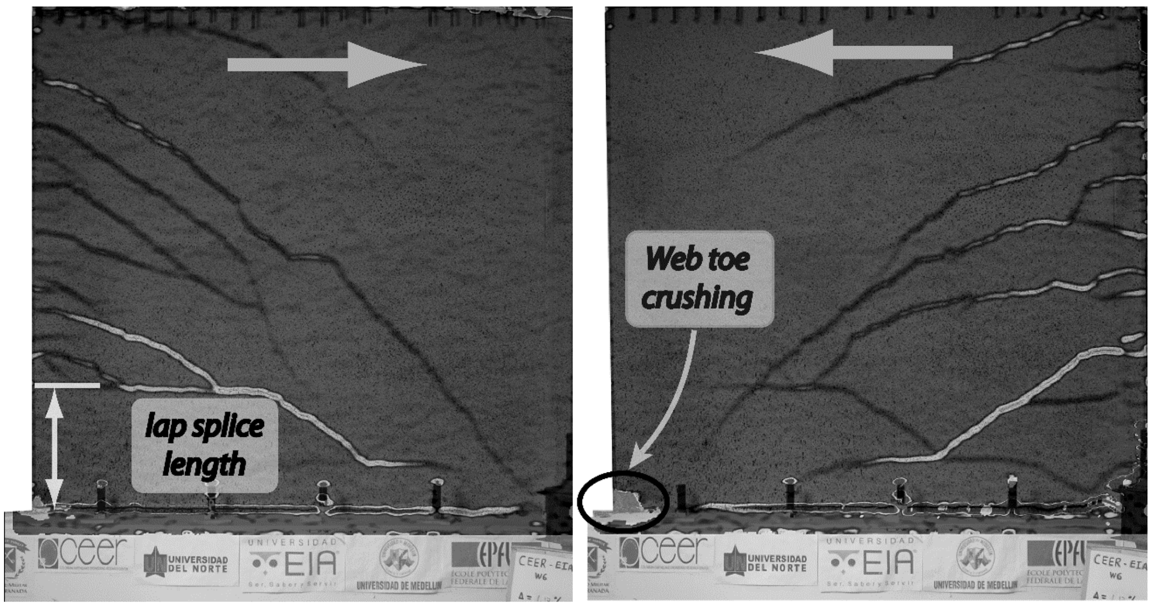

Figure 7. Cracking pattern at end of test of specimen W6: (a) flange compression cycles (left), (b) flange tensile cycle (right). The plot shows the vertical strains as computed by the DIC software. The patter revealed by the DIC software does not represent the crack width but a region of large strains around the crack.

Cracking propagation of specimen W7 was similar to that of specimen W6 for the half-cycles that compressed the edge with the short flange. Cracks on the flange side were evenly distributed along the height with wider cracks spreading towards the compressed toe at 0.7 m and 1.1 m above the foundation. There was also a wide crack at the wall-foundation interface that appeared at early loading stages. Fracture of the 6.3 mm (#2) dowel bars was observed during the second load step of Δ_R=0.83% that induced compression in the flange and continued for Δ_R=1.16%

for both directions. The fracture of these dowel bars was followed by the rupture of the 12.6 mm (#4) dowel bar at the wall-foundation interface during the second cycle of the same drift at the side with the shortest flange. This fracture caused the failure of the specimen due to the loss of the lateral strength larger than 20%. The reinforcement showed an inclined fracture that could have been cause by several tensile compressive cycles that induced buckling (see Figure 8).

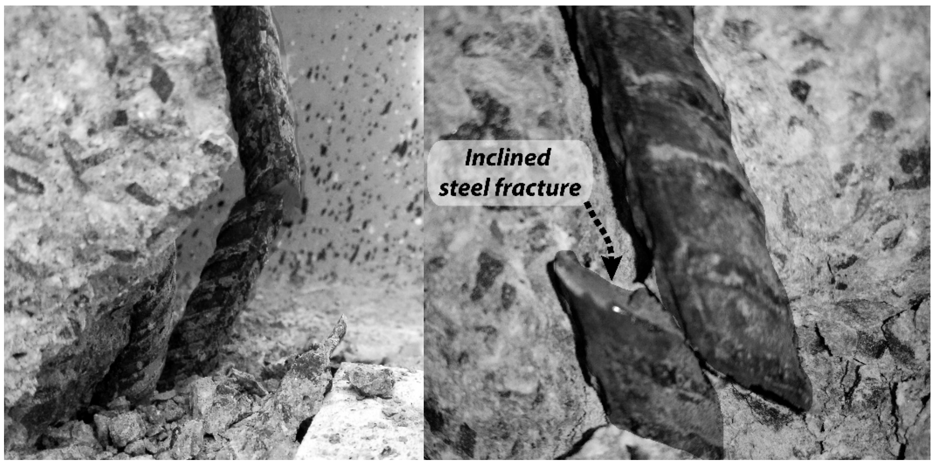

Figure 8. Reinforcement fracture at the shorter flange of specimen W7.

The evolution of cracking of specimens W5 and W6 is shown in Figure 9 for three different levels of drift ratio demand. Cracking extending more than half of the wall length, on the flange side of all the specimen, was observed for drift ratios as low as Δ_R= 0.17%. The entire crack pattern was completely developed at a drift ratio Δ_R= 0.42%. The cracks on the flange side (right hand side of the pictures) were well spread for all walls and remained approximately horizontal within the flange. The crack pattern for tensile flange cycles became then inclined along the web with angles varying between $16 \leq \theta_{cr} \leq 38$ degrees, with a typical inclination of approximately 35 degrees. On the other hand, crack pattern on the web-edge (left hand side of the pictures) differ among the walls. For instance, only a few wide cracks formed on units W4 and W5 (reinforced with the WWM) while a larger number of narrower cracks formed for specimens W6 and W7, due to the additional reinforcement placed at the web edge (W6) or at the shorter flange (W7).

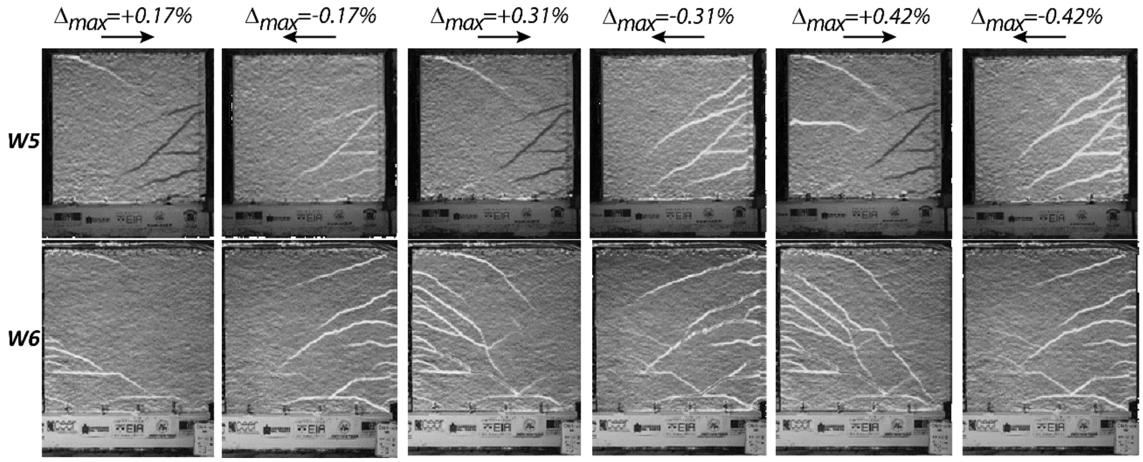

Figure 9. Evolution of crack propagation for specimens W5 and W6 at three different drift ratios. Pattern reveals regions of large vertical strains around the cracks and not the actual crack width.

3.2 Hysteretic response

Hysteretic curves are fundamental indicators of the global strength and deformation capacities as well as other important parameters such as stiffness degradation and energy dissipation [37]. The hysteretic curves of the walls are shown in Figure 10. They are expressed in terms of lateral force and lateral drift ratio. To account for different values of concrete strength (f'_c), the ratio between the shear stress and the square root of f'_c ($\sqrt{f'_c}$) is also shown in the figure. The shear stress was computed as the ratio between the lateral force and the gross area of the wall web ($L_w t_w$).

As shown in Figure 10a, specimen W4 showed a stepped strength degradation after a lateral drift of +0.61% when the 6.3 mm (#2) dowel bars started rupturing at the wall-foundation interface during the load step that induced compression in the flange. After a sudden strength drop at +0.75% drift, the load was reversed and a lateral drift of -0.73% was reached before the strength started to decrease due to the crushing of the concrete at the bottom web edge. As shown in Figure 10b, the specimen W5 was able to reach a drift of +0.69% during a load step inducing web tension before strength started to decrease due to rupture of the 6.3 mm (#2) dowel bars at the web side. The specimen W5 reached a maximum drift of +1.10% for the flange compression load step and -1.20% for the flange tensile load step before the fracture of most of the dowel bars and the crushing onset of the web edge concrete. However, the strength degradation for those drift levels was approximately 42% and 31%, respectively. A 20% of strength degradation, which is commonly used as a criterion for failure, was observed at Δ_R=+0.80% and Δ_R= -0.97% for compressive and tensile flange load steps, respectively. Specimen W6 showed more stable loops with strength degradation lower than 13% during the second loading cycle for a lateral drift close to ±0.85% in both directions (Figure 10c). A sudden strength drop occurred at Δ_R=+0.92% during the flange compression load steps due to the failure of the lap splice of the 12.6 mm (#4) reinforcing bars at the web edge. At that instant, the strength degradation reached 16%. The hysteretic response of specimen W7 was similar to that of specimen W6 up to a lateral drift of Δ_R=±0.85%. As shown in Figure 10d, the specimen W7 was able to accommodate two additional cycles up to Δ_R=1.20% but suffered a strength degradation larger than 35% at this point. A 20% strength degradation was observed for a drift ratio close to +1.15% for the flange compressive cycle and -1.24 for the flange tensile cycle.

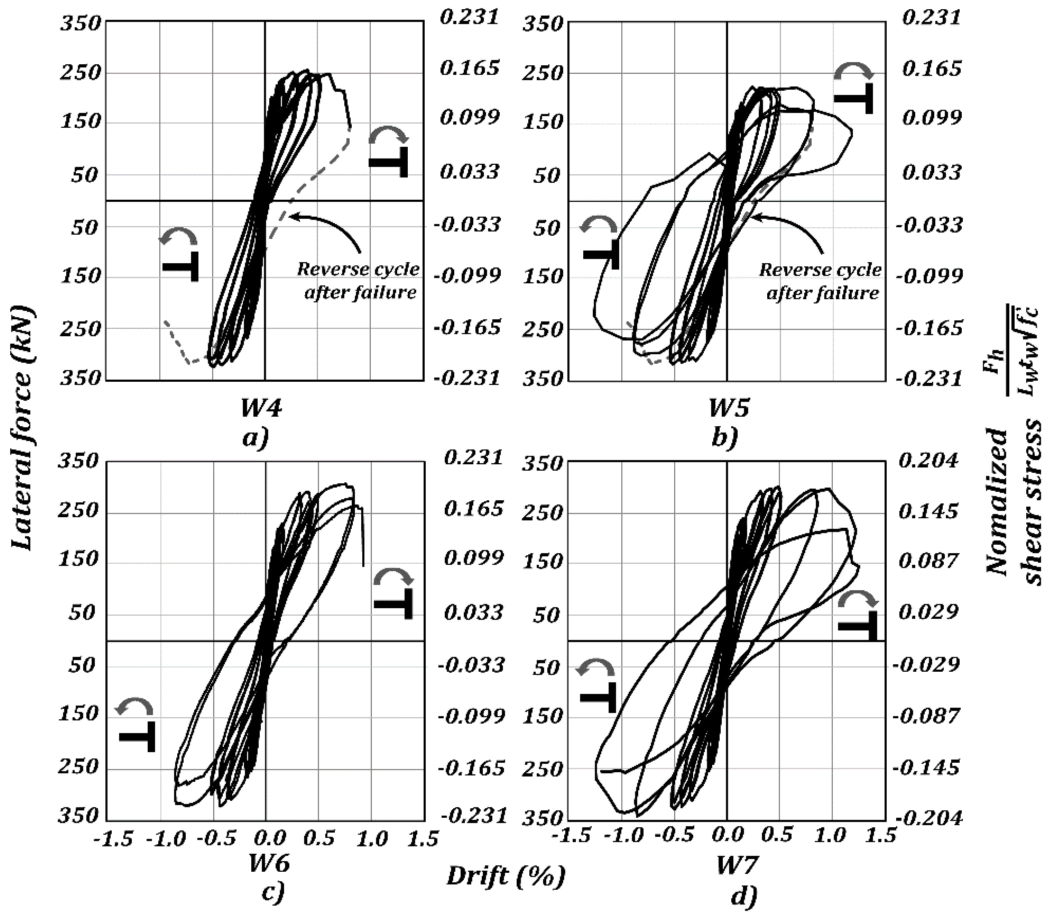

Figure 10. Drift ratio versus base shear relationships for walls W4, W5, W6, and W7.

For special RC structural walls, ACI 318 [2] prescribes that the relative contribution of concrete to nominal wall shear strength is $0.17\sqrt{f_c^{'}}$MPa for walls with H/Lw equal or higher 2.0. As shown in Figure 10, the peak strength of wall specimens varied between 0.14 $\sqrt{f_c^{'}}$ MPa for W5 and 0.21 $\sqrt{f_c^{'}}$ MPa for W6 during the flange compression cycles. These peak strength values close or lower than the contribution of concrete to wall shear strength indicate a limited shear contribution to the total response.

4. Analysis and discussion of results

The response of the specimens is compared next with regard to their drift capacity at certain limit states, their backbone force-displacement envelopes, the contributions to the drift from flexural, shear and sliding deformations, and the evolution of stiffness degradation and energy dissipation.

4.1 Limit states

To identify key parameters of the behavior of the walls, five performance levels were defined on the envelope of the hysteretic response as follows: cracking moment (CM), first yield at the base crack (YBC), first yield above the base crack (YABC), peak lateral resistance (PLR), and loss of lateral resistance (LLR).

The CM limit state defines the drift range over which the in-plane stiffness of the wall panel is largest. Additionally, for lightly reinforced wall panels where the yielding moment may be close to the cracking moment, the CM limit state definition may help detective the potential of a brittle failure (e.g. if cracking moment is larger than the yielding moment). The CM limit state was theoretically defined by computing the cracking moment, M_{cr}, of the cross section using Eq. (1).

$$\boldsymbol{M_{cr}} = \frac{(f_r + P/A_g)I_g}{y} = \frac{(0.62\sqrt{f_c^{'}} + P/A_g)I_g}{y} \tag{1}$$

where y is the distance from the centroid to the extreme fiber in tension, A_g and I_g are the gross area and gross moment of inertia of the cross-section, respectively, and f_r is the modulus of rupture of the concrete, which is defined in terms of the compressive strength, $f_c^{'}$ (MPa), at the day of the test following NSR-10 provisions. The base shear force associated to the CM limit is estimated using the shear span ratio M_u/V_uL_w of the experiments, which as stated was kept constant at 2.08 for all tests.

For slender reinforced concrete walls with low axial load, one of the main contributions to the total displacement comes from rigid body rotation around the neutral axis, due to the crack at the wall-base interface [38]. Furthermore, the impact of the base-crack opening on total displacement is greater for lightly reinforced panels [39]. The YBC limit is defined based on the strain penetration model presented by Moehle [40]. Such model relates slip deformation due to rigid-body rotation with both the geometry and stress state of the reinforcing bars at the edge of the panels in the interface with the foundation. The model assumes that the tension force in the bar gradually decreases from the maximum stress demand at the wall-base interface ($f_{s,max}$), to zero stress at the anchorage distance into the base. Bar elongation (s_a) from this point to the wall-base interface can be computed as the integral of the strain along the anchorage length (l_a). If $f_{s,max} = f_y$ (i.e. YBC limit is reached), s_a can be estimated using Eq. (2):

$$\boldsymbol{s_a = \frac{f_y^2 d_b}{8E_s\bar{u}}} \tag{2}$$

where d_b is the bar diameter, E_s = 200 GPa is the elastic modulus of steel, and $\bar{u} = 1.0\sqrt{f'_c}$ (MPa) is the average uniform bond stress recommended by ACI 363-92 [37] for linear response (i.e. up to $f_{s,max} = f_y$). The YBC limit is met when the theoretically computed s_a values reach the experimental measurements recorded with the displacement transducers near the base (32 and 15). The short gage length of these transducers (e.g. 50 mm) ensures that the recorded displacements only account for crack opening at the base without much contribution from strains above the crack.

The YABC limit state is set by determining the test step in which the rebar elongation (ds_{tr}), measured with the transducers located along the edges of the wall, exceeded the yield strain limit. The strain in the bars at the i-th location along the height of the panel was estimated as $\varepsilon_{Str,i} = ds_{tr,i} / L_{tr,i}$ where is the $L_{tr,i}$ is the gage length of the i-th transducer. This value was compared against the yield strain of each bar in at the edge of the panel (i.e. $\varepsilon_y = f_y/E_s$). The PLR limit state is related to the peak load for each loading direction and was directly obtained from the hysteresis response. For code-based seismic design, the LLR limit state is reached when a loss of 20% in capacity is observed after the peak shear strength is achieved.

Figure 11 shows the backbone curves enveloping the previously presented hysteresis loops, marking the limit states previously described. For the direction compressing the web edge, the response of specimens W4, W5 and W6 was similar. This is expected because the specimens had the same cross-section geometry, and the response in this direction is mainly commanded by the tensile strength of the reinforcement in the flange, which was the same in this set of specimens. The envelope for specimen W7 exhibits a larger capacity in strength and displacement due to the enlarged element at the web edge.

The response for the direction compressing the flange is dependent on the reinforcing characteristics of the specimens. Specimens W6 and W7 reached the largest capacity among all specimens thanks to the two additional 13 mm bars at the web edge. Furthermore, specimen W7 exhibited the largest displacement capacity of the four units. Although specimen W5 was expected to reach a higher strength as compared to W4 because of the larger yield strength of the WWM, its capacity was 12% lower. This could be in part because the reinforcement details and the type of steel at the foundation-wall interface, where most of the plastic deformations occurred, is similar for both units.

Drift ratios at defined limit states are shown in Table 2. For the direction compressing the web edge, the DCR limit is reached in the drift range $0.024 \leq \Delta_R \leq 0.033\%$ for specimens W4, W5 and W6, and at $\Delta_R = 0.041\%$ for specimen W7. For the opposite direction, the DCR limit is reached in the range $0.017 \leq \Delta_R \leq 0.024\%$ for specimens W4, W5 and W6, and at $\Delta_R = 0.032\%$ for W7. The YBC limit was also reached early on in the loading sequence. In both loading direction, all specimens reached the YBC limit in the range $0.08 \leq \Delta_R \leq 0.10\%$, except for specimen W5 who reached at 0.03% drift when compressing the flange. The limited cracking drifts values discussed above should be considered in newer revisions of the Colombian Building Code, NSR-10, to prescribe the use of non-cracked moments of inertia when analyzing the seismic action on multistory wall structural systems.

Specimen W5 did not reached the YABC limit when compressing the flange, indicating that most of the plastic deformation on the edge rebar was concentrated at the base crack. Additionally, the lack of strain hardening of the WWM on the web prevented the spread of the plasticity along the web edge. The YABC limit was recorded at 0.09, 0.24 and 0.14% drift ratio for specimens W5, W6 and W7, respectively. For the opposite direction, the YABC limit was achieved between 0.19 and 0.29% drift ratio for all specimens. When compressing the flange, the specimen W5 reached its maximum strength at the smallest drift ratio (i.e. Δ_R = 0.32%) among all specimens. This value is 27% smaller than that of specimen W4. Past this point, the force-displacement backbone of specimen W5 remained flat up to the onset of strength loss at Δ_R = 0.32%. Specimen W6 and W7 reached the maximum strength close to 0.80% drift ratio in both directions.

For the direction compressing the flange, the displacement capacity at the LLR limit of specimens W6 was 15% and 56% larger than that of specimens W4 and W5, respectively. This result shows the benefits of the additional ductile reinforcement at the web edge, which provoked an increase in both, the strength and displacement performance of the panels. The displacement capacity of specimen W7 was 25% larger than that of W6. For the direction compressing the thin web edge, the displacement capacity of specimen W7 was at least 17% larger than that of any other specimen, evidencing the beneficial effect of the enlarged boundary.

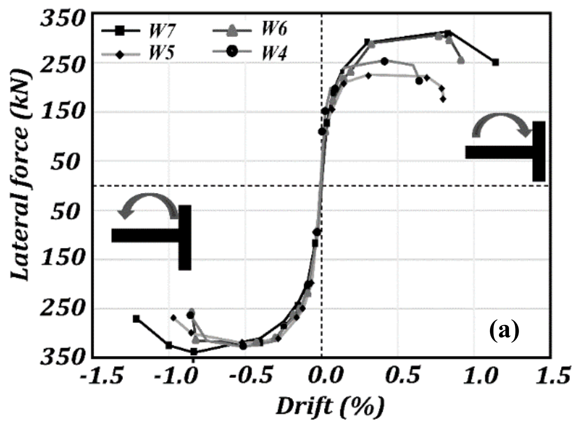

Figure 11. Backbone curves of all specimens.

Table 2. Drift ratios at defined limit states.

Limit State	Drift at defined limit states (%)							
	W4		W5		W6		W7	
	FCC*	FTC*	FCC	FTC	FCC	FTC	FCC	FTC
DCR	0.025	-0.024	0.024	-0.017	0.033	-0.020	0.041	-0.032
YBC	0.08	-0.08	0.03	-0.10	0.08	-0.08	0.08	-0.10
YABC	N.R.	-0.19	0.09	-0.26	0.24	-0.21	0.14	-0.29
PLR	0.32	-0.49	0.44	-0.58	0.76	-0.79	0.85	-0.85
LLR	0.59	-1.06	0.80	-0.87	0.92	-0.86	1.15	-1.24

*FCC: Flange compression loads step. FTC: Flange tensile load steps.
N.R: limit state Not Reached.

4.2 Deformation components

The sources of wall deformation were identified based on the recordings from the different sensors located on the walls (see Figure 12). Four different deformation components were identified: (i) contribution of rocking or the rotation along the wall foundation, (ii) flexural deformations due to the spreading of plasticity along the wall, (iii) web shear and (iv) sliding at the base. The contribution of the four deformation components to the total drift at the PLR limit state is shown in Figure 12. The rotation along the wall-foundation interface crack involved the largest contribution as it reached 42.8%, 64.5%, 44.1% and 37.3% of the total displacement contribution for specimens W4, W5, W6 and W7, respectively. Displacements of unit W5 when compressing the flange are therefore mainly due to rigid body rotation, which is consistent with the absence of yielding above the base crack. The flexural contribution to the total deformation was 42.8% for W4, 24.6% for W6, 27.7% for W7 and was negligible for W5 as most of the rotation was concentrated at the foundation-wall interface and only one observable crack formed along the wall height. Shear deformation, calculated according to Hiraishi [41], had no significant contribution to total deformation of specimens W4 and W5; however, shear deformation contributed 25.9% and 22.9% to the total deformation for specimens W6 and W7, respectively. This increase of shear deformations is explained by the increased number of cracks along the web in these specimens, which were not observed in specimens W4 or W5. Sliding along the base was not significant for any of the walls as contributions were lower than 7%.

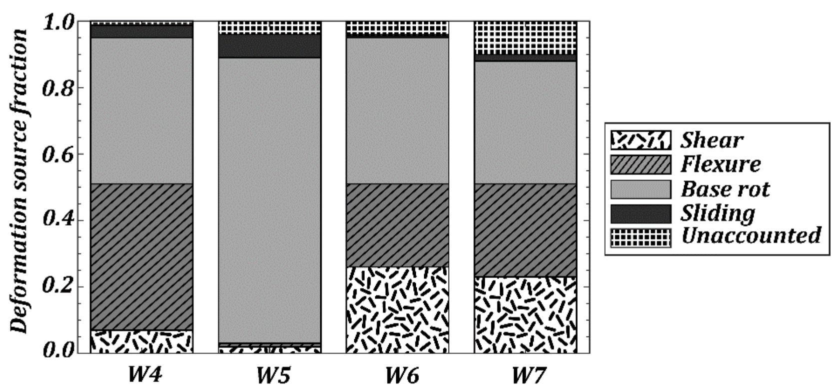

Figure 12. Contribution of deformation components to the total displacement for the PLR limit state in the direction that compresses the flange.

The base rotation drift is compared to the total drift when compressing the flange in Figure 13 for three limit states: DCR, YABC and PLR. As previously discussed, the rocking at the wall-foundation interface was the main contributor to the total displacements in view of the low longitudinal reinforcing ratio of the specimens. Such rocking induced a crack along the interface and subsequent large strains of the dowel bars connecting the wall to the foundation. The rotation from the base crack was largest for specimen W5 (with the WWM) at any instant of the experiment. This is consistent with the scarcity of cracks along the height of the web edge (see Figure **Error! Reference source not found.**). On the other end, specimens W6 and W7 exhibited the smallest rigid body contribution to the total displacement greatly due to the additional reinforcement at the web edge, which prevented a wider crack opening, and facilitated the spread of plasticity along the web edge.

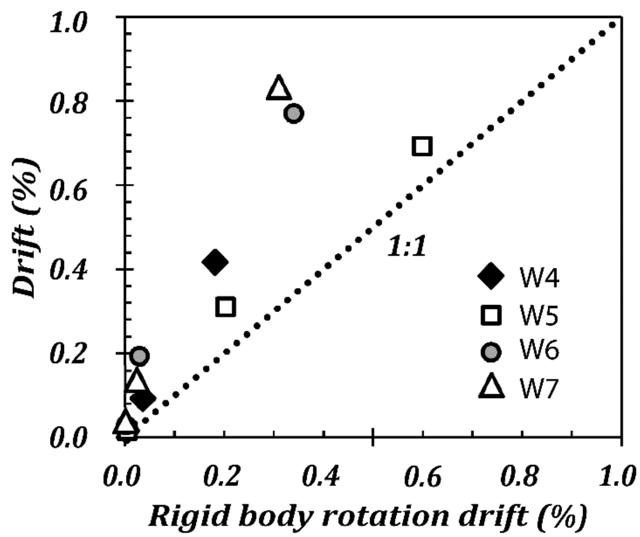

Figure 13. Evolution of base rotation contribution to total drift.

4.3 Out-of-plane deformation

The instrumental and video recordings taken at the web edge for specimens W4 to W6 showed that the out-of-plane displacement (OPD) of the specimens was negligible, hence no signs of wall buckling were observed. Maximum OPD normalized by wall thickness (OPD/t_w) was smaller than 0.085, being larger for specimen W4. The tensile strain applied prior to subsequent loading in compression is the parameter that governs the out-of-plane instability [42]. As shown in Table 3, the maximum total strain along the web edge recorded from the cycles that put the web edge in tension was lower than 1%. Additionally, if the contribution of the base crack is not accounted for in this average strain calculation, the maximum strain above the base crack did not exceed 0.4%. This low strain values above the wall-foundation interface have likely prevented the occurrence of relevant out-of-plane deformations. According to Eq. (4) from Parra and Moehle [25] the critical tensile strain ($\xi_{sm,cr}$) that would induce out-of-plane failure would be around 1.6% for the walls with no additional end reinforcement (W4 and W5) and around 1.1% for the wall with the additional 12.5 mm (#4) reinforcement bars at the wall end (W6). As one the wall had only one reinforcement layer κ was defined as 0.5, the wall was assumed to have perfect fix at the top and bottom beams, and therefore k was defined as 0.5. The wall thickness (b_{cr}) used was 100 mm and the wall clear height (h_u) was 2400 mm.

$$\xi_{sm,cr} = \kappa \xi_{cr} \left(\frac{\pi b_{cr}}{k h_u} \right)^2 + 0.005 \tag{3}$$

$$\xi_{cr} = 0.5 \left(1 + \frac{2m}{0.85} - \sqrt{\left(\frac{2m}{0.85} \right)^2 + \frac{4m}{0.85}} \right)$$

$$m = \rho \frac{f_y}{f_c'}$$

Table 3. Maximum strain during load stages inducing tensile cycles at the web edge.

Specimen	W4	W5	W6	W7
Average strain over wall height at web edge (mm/mm)	0.010	0.007	0.008	0.010
Average strain if opening of base crack is excluded (mm/mm)	0.003	0.002	0.004	0.004
Drift (%)	+0.96	+0.86	+0.83	+1.14

4.4 Stiffness degradation

The stiffness degradation curve is commonly related with the increase of the deformation demand of the element. For practical earthquake-resistant design, deformation is commonly expressed in terms of story drift ratio and the stiffness degradation in terms of the ratio of the stiffness of a particular cycle and the stiffness of the first cycle or initial stiffness (K_e/K_i). Using the latter approach, stiffness degradation curves of the test units are shown in Figure 14. Trends of stiffness degradation demonstrated that walls experienced a rapid degradation as the reduction of the initial stiffness was close to 70% ($K_e/K_i \approx 0.3$) for drift ratios between 0.16% and 0.25% for the flange tensile cycles, and between 0.09% and 0.15% for the flange compressive tests. At 1% drift ratio, which is considered a design limit according to the local design guidelines when uncracked sections are considered in the design process, the effective stiffness was lower that 10% of the initial stiffness (K_e/K_i = 0.1) for all the specimens. These results indicate the significance of considering the cracked sections in the design process as drift may be significantly underestimated if gross sections are used to verify drift limits defined by the Colombian code [1]. Table 4 shows values of stiffness degradation (K_e/K_i) to each of the defined limit states for all the specimens.

Table 4. Stiffness degradation ratios at defined limit states.

Limit State	Stiffness degradation at defined limit states (%)							
	W4		W5		W6		W7	
	FCC	FTC	FCC	FTC	FCC	FTC	FCC	FTC
DCR	0.87	0.99	0.78	0.96	0.69	0.98	0.71	0.82
YBC	0.69	0.44	0.34	0.64	0.44	0.64	0.52	0.48
YABC	0.33	0.23	N.A.*	0.35	0.23	0.34	0.33	0.24
PLR	0.09	0.11	0.13	0.15	0.07	0.09	0.08	0.09
LLR	0.04	0.06	0.06	0.06	0.03	0.08	0.05	0.05

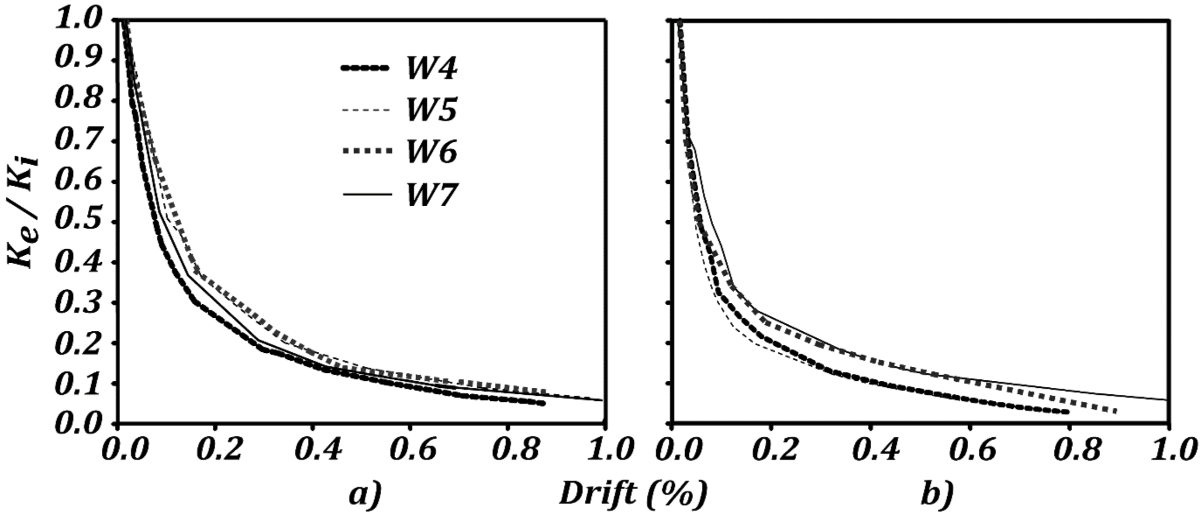

Figure 14. Stiffness degradation of walls: (a) flange tensile cycles, (b) flange compressive cycles.

4.5 Energy dissipation

The energy dissipated is a crucial seismic-performance parameter for structural elements subjected to several loading cycles. The variation of dissipated energy versus drift ratio is shown in Figure 15a. The elastic energy was obtained as the area below the lateral force vs displacement envelope for each load step and the dissipated energy was obtained as the total area inside the hysteresis loop. As shown in Figure 15a, the specimen W5 experienced the largest amount of dissipated energy up to a drift of 0.57%. After this drift, W4 shows the largest dissipated energy. The reinforcement of specimen W4 included moderate ductility reinforcement mesh and no additional reinforcement at the ends while W5 had the low ductility steel mesh. On the other hand, the specimen W6 and W7 experienced the lowest energy dissipation. Specimen W6 was reinforced with a moderate ductility reinforcement mesh and additional reinforcement bars at the wall end while W7 had flanges at the two ends. Wall W6 experienced a lap splice failure and W7 had reinforcement fracture at both ends. At a drift ratio of 0.7%, W6 reached just 61% of the energy dissipated by W4 and 73% of the energy dissipated by W5. W7 dissipation was lightly smaller which may indicate that the even if the concentrated reinforcement at the wall ends improves the crack distribution; it does not necessarily improves the energy dissipation.

The ratio of dissipated and elastic energy is included in Figure 15b. As shown in the figure, specimen W4, W6 and W7 showed a rapid decrease of the relative dissipated energy up to a drift ratio of approximately 0.1%. After that decrease, a slight to moderate increase and a relatively constant region was observed up to a drift ratio of roughly 0.5%. For drift ratios larger than 0.5%, the relative energy increases with the drift ratio but at a faster rate. On the other hand, specimen W5 also experienced an initial decrease of ratio of dissipated energy; however, a relatively constant rate of increase was observed up to the maximum drift recorded. The behavior for W5 may be due to the limited cracking during the first cycles that increased gradually during the test. The limited cracking produced a smaller dissipated energy compare to the elastic energy but this dissipation gradually increased as a couple of cracks opened along the wall at the web side.

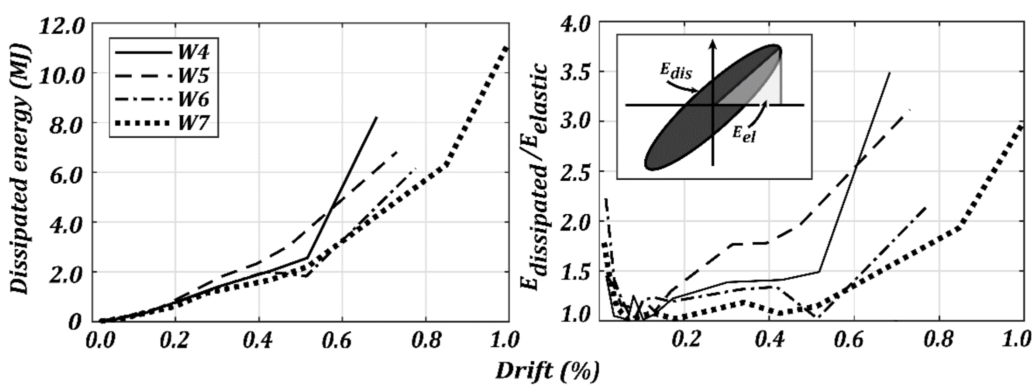

Figure 15. Energy dissipation: (a) dissipated energy (left), (b) relative dissipated energy (right).

5. Comparison with plausible displacement demand at the design level

Results of linear response history analyses over 15 multistory thin-wall buildings from Arteta [11] are adapted next to correlate demand and capacity of thin walls buildings in Colombia. The models were selected from a Colombian building database comprising structures with 4 to 18 stories in height (i.e. 10 to 43 m in height). The median value of the Sozen [43] wall-area index (ratio between area of wall-webs in a given direction and the first floor area) for these buildings is 3.7%, with minimum and maximum values of 1.4 and 9.8%, respectively. Most of the structures evaluated (approximately 70%) have wall-area index larger than 3%, which are considered "robust", and safe under seismic shaking. Further details of the building set geometry, and their dynamic characteristics can be found in [3].

Figure 16a shows the maximum roof drift ratio (RDR) demand versus cracked period relationship in the longitudinal direction of the structure. Each model is represented by its structural period and was analyzed under a set of 11 two-horizontal-component ground motions, selected such that the median of their geomean spectra matched the design level of the code-based spectrum. A power regression for the median and the 84th percentile demand is depicted along with the individual response. The upper and lower bound of drift capacity at the LLR-limit, of the panels presented herein, in the direction compressing the flange, are traced as horizontal dotted lines. It is noted that the lower bound capacity is exceeded at the median and 84th percentile level for structural periods larger than 1.10 s and 0.85 s, respectively. This period range is covered by structures with more than 14 stories, which represent one-third of the buildings in the database. It is worth emphasizing that the elastic models do not account for flexural yielding of the critical cross sections, and hence, the results presented above might not be conservative.

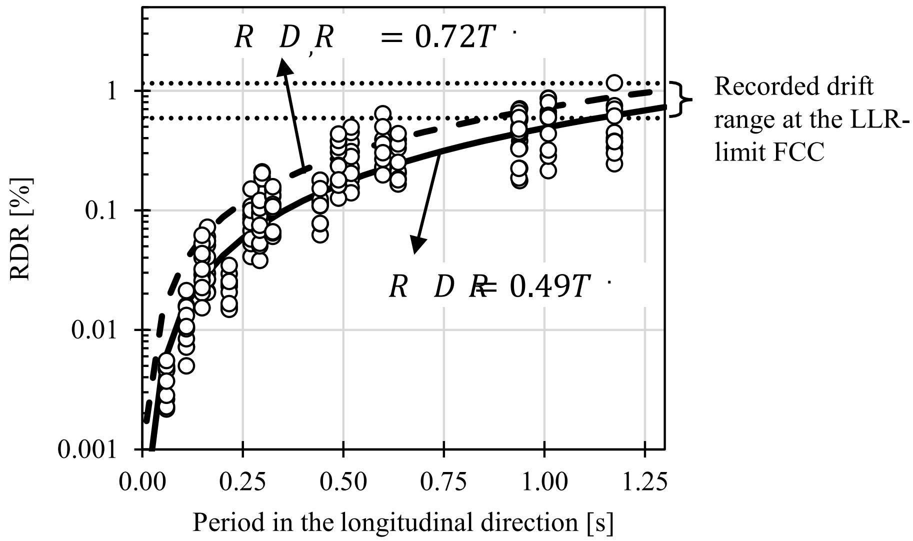

Figure 16. Displacement demand at the design level for Colombian thin-wall RC buildings: roof-drift-ratio versus cracked period.

6. Conclusions

Four full-scale thin reinforced concrete walls were built and tested to evaluate their performance under lateral cyclic loading. These units were aimed to represent the current local practices for one of the typical construction systems used in Colombia and were defined based on the analysis of a database of buildings from 8 to 15 stories with low axial load ratios (below 5%) and light steel reinforcement ratios along the web. The tested specimens variables as wall length, shear span ratio and additional steel at the wall edges are representative of the database. However, walls with different characteristics are also common within the database.

The results from all the specimens showed a limited deformation capacity well below 1.43% which is the maximum drift limit specified by the code for buildings designed based on cracked sections. Hence, these walls would not be able to perform according to the code requirements if included in buildings allowed to reach the maximum drift limit. Significant lower design drift limits should be used if this type of walls are to be included as part of the lateral resisting system of the building.

In terms of the failure mode, the walls were characterized by the rupture of the steel, mainly due to the concentration of plasticity in a single crack located at the wall-foundation interface. This concentration was more evident when a low ductility cold-drawn welded mesh was used as web reinforcement, instead of deformed bars with moderate ductility. Lap splice failure mode due to bar slippage was also observed which induced a significant decrease of the energy dissipation compared to the steel rupture failure mode.

In terms of the displacement capacity of the walls, a slight increase was obtained by providing additional reinforcement with moderate ductility at the wall ends as these improved the crack distribution along the wall height. Additional displacement capacity was obtained by adding the short flange in W7 as it prevented the lap splice failure that occurred in W6. There was no evidence of buckling of the wall under load steps that induced compression on the web, possibly due to the limited elongation along the web edge, above the base crack. Stiffness degradation curves demonstrated that walls experienced a rapid deterioration as the loss of the initial stiffness was roughly equivalent to 50%, 85%, 90% for drift ratios close to 0.1%, 0.5% and 0.7%, respectively. Such critical values of stiffness degradation evidenced that typical cracking factors proposed by the local building code, which are significantly higher, cannot be used for code-based seismic design of walls with similar characteristics to those tested. Results of this study are applicable only to walls with conditions similar to those reported here. Future experimental programs should consider variations on the axial load ratio and the impact of heavily reinforced web boundaries as this may trigger other failure modes such as out-of-plane instability or early concrete crushing.

A case study with a set of linear elastic response history analyses of multistory buildings, representative of the construction practice of thin-wall buildings in Colombia, showed that the roof drift ratio demand at the design level of demand, might exceed the capacity of the walls tested, specifically for structures taller than 14 stories.

Acknowledgments

The research was financed through an *EPFL Seed Money* grant through the Ecole Polytechnique Fédérale de Lausanne (EPFL) *Cooperation and Development Center* in Switzerland and additional funding was provided by Conconcreto. The authors would like to thank Wilson Zapata, Julian del Rio Echeverri, and Juan Fernando Garcia from Conconcreto for the logistic support and technical advice. Special thanks go to: Gustavo Araujo and Julio Sánchez from UNINORTE for the hard work in the laboratory and reducing the experimental data and Juan Carlos Velez from Universidad de Antioquia for the laboratory assistance, to Jose Fernando Rave, Javier Penagos, Juanita Escobar, Juan David Upegui and Jonathan Betancur at EIA University for the long hours preparing the specimens, and to Juan Fernando Restrepo and Julián Ossa at University of Medellín for their assistance in the laboratory. Finally, the authors thank Mauricio Ramirez from DAQ Solutions for providing the required assistance to complete the tests. Authors expresses their gratitude to EIA, UNINORTE, UDEM and UMNG universities for supporting research activities of the first four authors.

References

[1] NSR-10, Colombian code for earthquake-resistant construction, NSR-10, Committee 100, Colombian Association of Earthquake Engineering, AIS, Colombia, 2010.

[2] ACI 318-08, Building code requirements for structural concrete and commentary. Committee 318. Farmington Hills, MI, American Concrete Institute; 2008. p. 467.

[3] Arteta, C. A., Sanchez, J., Daza, R., Blandón, C. A., Bonett, R. L., Carrillo, J., & Velez, J. C. Global and local demand limits of thin reinforced concrete structural wall building systems. In: Proceedings of the 16th World Conference on Earthquake Engineering, Santiago, January 9-13,. 2017, Paper 2121.

[4] Arteta, C. A., To, D. V., & Moehle, J. P. Experimental response of boundary elements of code compliant reinforced concrete shear walls. In: Proceeding of the 10th US National Conference on Earthquake Engineering, Earthquake Engineering Research Institute, Anchorage, AK, July 21-25 2014.

[5] Westenenk, B., de la Llera, J. C., Jünemann, R., Hube, M. A., Besa, J. J., Lüders, C., Jordán, R. Analysis and interpretation of the seismic response of RC buildings in Concepción during the February 27, 2010, Chile earthquake. Bulletin of Earthquake Engineering 2013; 11(1): 69-91. doi:10.1007/s10518-012-9404-5

[6] Gonzales, H., & López-Almansa, F. Seismic performance of buildings with thin RC bearing walls. Engineering Structures 2012; 34: 244-258, doi.org/10.1016/j.engstruct.2011.10.007

[7] Wallace, J. W., & Orakcal, K. ACI 318-99 provisions for seismic design of structural walls. ACI Structural Journal 2002; 99(4): 499-508, doi:10.14359/12119

[8] Alarcon, C., Hube, M. A., Junemann, R., & De la Llera, J. C. Characteristics and displacement capacity of reinforced concrete walls in damaged buildings during 2010 Chile earthquake. Bulletin of Earthquake Engineering 2015; 13(4): 1119-1139. doi:10.1007/s10518-015-9727-0

[9] Sri Sritharan, Katrin Beyer, Richard S. Henry, Y. H. Chai, Mervyn Kowalsky, and Desmond Bull (2014) Understanding poor seismic performance of concrete walls and design implications. Earthquake Spectra 2014, 30(1):307-334.

[10] Kam, W.Y., Pampanin, S. and Elwood, K. Seismic performance of reinforced concrete buildings in the 22 February Christchurch (Lyttelton) earthquake. Bulletin of the New Zealand Society for Earthquake Engineering 2011; 44(4):239-278.

[11] Arteta, C. A. Simple mechanics of reinforced concrete thin wall, design considerations for Colombia. In: Proceedings of the VIII National Conference on Earthquake Engineering, Barranquilla, Colombia 2017, paper 1750.

[12] Rosso, A., Almeida, J. P., & Beyer, K. Stability of thin reinforced concrete walls under cyclic loads: State-of-the-art and new experimental findings. Bulletin of Earthquake Engineering 2016; 14(2): 455-484, doi:10.1007/s10518-015-9827-x

[13] Almeida, J., Prodan, O., Rosso, A., & Beyer, K. Tests on thin reinforced concrete walls subjected to in-plane and out-of-plane cyclic loading. Earthquake Spectra 2017; 33(1): 323-345. doi:10.1193/101915eqs154dp

[14] Rosso, A., Jiménez-Roa, L. A., de Almeida, J. P., Guerrero, A. P., Blandón, C. A., Bonett, R. L., & Beyer, K. Cyclic tensile-compressive tests on thin concrete boundary elements with a single layer of reinforcement prone to out-of-plane instability. Bulletin of Earthquake Engineering 2018; 16: 859, doi:10.1007/s10518-017-0228-1

[15] Rosso, A., Jiménez-Roa, L. A., de Almeida, J. P. & Beyer, K. Instability of thin concrete walls with a single layer of reinforcement under cyclic loading: Numerical simulation and improved equivalent boundary element model for assessment, Journal of Earthquake Engineering (under review), 2018.

[16] McMenamin, A., The performance of slender precast reinforced concrete cantilever walls with roof level lateral displacement restraint under simulated in-plane seismic loading, Research Report 99-4, Department of Civil Engineering, University of Canterbury, Christchurch, New Zealand, 1999, 275p.

[17] Carrillo, J. & Alcocer, S. Experimental investigation on dynamic and quasi-static behavior of low-rise reinforced concrete walls. Earthquake Engineering and Structural Dynamics 2013; 42: 635-652. doi:10.1002/eqe.2234.

[18] Tomazevic, M., Lutman, M., Capuder, F., & Petkovic, L. Seismic Behaviour of R.C. Shear-Walls: An Experimental Study, 11th World Conference on Earthquake Engineering, Paper 381, Elsevier, 1996, ISBN: 0080428223

[19] Massone, L., Bonelli, P., Lagos, R., Lüders, C., Moehle, J., & Wallace, J. W. Seismic design and construction practices for RC structural wall buildings. Earthquake Spectra 2012, 28(S1): S245-S256. doi:10.1193/1.4000046

[20] Thomsen, J. H., & Wallace, J. W. Displacement-based design of slender reinforced concrete structural walls-experimental verification. Journal of Structural Engineering 2004; 130(4): 618-630. doi:10.1061/(Asce)0733-9445(2004)130:4(618)

[21] Wallace, J. W., Massone, L. M., Bonelli, P., Dragovich, J., Lagos, R., Luders, C., & Moehle, J. P. Damage and implications for seismic design of RC structural wall buildings. Earthquake Spectra 2012; 28(S1), S281-S299, doi:10.1193/1.4000047

[22] Blandón, C. A., Rave-Arango, J. F., & Bonett, R. L. Behavior of thin reinforced concrete walls under lateral load. In: Proceedings of the VII National Conference on Earthquake Engineering, Bogota, 2015, Paper 25.

[23] Goodsir, W. J. The design of coupled frame-wall structures for seismic actions. University of Canterbury, Christchurch, New Zealand, 1985.

[24] Hube, M. A., Marihuen, A., De la Llera, J. C., & Stojadinovic, B. Seismic behavior of slender reinforced concrete walls. Engineering Structures 2014; 80:377–388, doi:10.1016/j.engstruct.2014.09.014.

[25] Parra, P. F., & Moehle, J. P. Stability of slender wall boundaries subjected to earthquake loading. ACI Structural Journal 2017; 114(6):1627-1636.

[26] Dazio, A., Beyer, K. and Bachmann, H. Quasi-static cyclic tests and plastic hinge analysis of RC structural walls. Engineering Structures 2009; 31:1556-1571.

[27] Haindl, M., Hube, Matías A, & Arteta, C.A. Seismic performance assessment of a reinforced concrete wall house. VII National Conference on Earthquake Engineering, Bogota, 2015, Paper 23.

[28] Quiroz, L. G., Maruyama, Yoshihisa, & Zavala, Carlos. Cyclic behavior of thin RC Peruvian shear walls: Full-scale experimental investigation and numerical simulation. Engineering Structures 2013: 52: 153-167, doi.org/10.1016/j.engstruct.2013.02.033.

[29] Su, R. K. L., Wong, S. M., Seismic behaviour of slender reinforced concrete shear walls under high axial load ratio, Engineering Structures 2007; 29(8):1957-1965. doi:10.1016/j.engstruct.2006.10.020.

[30] Alarcon, C., Hube, M. A., & de la Llera, J. C. Effect of axial loads in the seismic behavior of reinforced concrete walls with unconfined wall boundaries. Engineering Structures 2014; 73:13–23, doi:10.1016/j.engstruct.2014.04.047.

[31] TNO Building and Construction Research. DIANA – Finite Element Analysis User's Manual. Release 8.1 September 2002.

[32] Chu, T. C., Ranson, W. F., Sutton, M. A., & Peters, W. H. Applications of digital-image-correlation techniques to experimental mechanics. Experimental Mechanics 1985; 25(3): 232-244, doi:10.1007/Bf02325092

[33] Pan, B., Qian, K. M., Xie, H. M., & Asundi, A. Two-dimensional digital image correlation for in-plane displacement and strain measurement: a review. Measurement Science & Technology 2009; 20(6):1-17. doi:Artn 062001

[34] Sutton, M. A., Orteu, J. J., & Schreier, H. W. Image correlation for shape, motion and deformation measurements: basic concepts, theory and applications. New York, NY: Springer, 2009.

[35] ASTM-A706. Standard specification for low-alloy steel deformed and plain bars for concrete reinforcement (pp. 6). West Conshohocken, PA: ASTM International, 2009.

[36] Almeida, J.P., Prodan, O., Tarquini, D., Beyer, K., Influence of lap splices on the deformation capacity of RC walls. I: database assembly, new experimental tests, and findings for model development. ASCE Journal of Structural Engineering 2017, 143(12).

[37] ACI Committee 363. Report on high-strength concrete. ACI Manual of Concrete Practice (reapproved 1997) (pp. 55). Farmington Hills, MI: American Concrete Institute, 1992.

[38] Lowes, L. N., Lehman, D. E., Birely, A. C., Kuchma, D. A., Marley, K. P., & Hart, C. R. (2012). Earthquake response of slender planar concrete walls with modern detailing. Engineering Structures, 43, 31-47. doi:10.1016/j.engstruct.2012.04.040

[39] Lu, Y., Henry, R. S., Gultom, R., & Ma, M. T. (2017). Cyclic Testing of Reinforced Concrete Walls with Distributed Minimum Vertical Reinforcement. Journal of Structural Engineering, 143(5), 04016225. doi:doi:10.1061/(ASCE)ST.1943-541X.0001723

[40] Moehle, J. P. Seismic design of reinforced concrete buildings. New York, NY: McGraw-Hill Professional, 2014.

[41] Hiraishi, H., Evaluation of shear and flexural deformations of flexural type shear walls. Bulletin of the New Zealand Society for Earthquake Engineering 1984, 17(2):135-144.

[42] Paulay T, Priestley MJN. Stability of ductile structural walls. ACI Structural Journal 1993, 90:385-392

[43] Sozen, M. A. Earthquake response of buildings with robust walls. Paper presented at the Fifth Chilean Conference on Seismology and Earthquake Engineering, Santiago de Chile, 1989.